Capillary filling in microchannels patterned by posts

B. M. Mognetti and J. M. Yeomans

The Rudolf Peierls Centre for Theoretical Physics, 1 Keble Road, Oxford OX1 3NP, United Kingdom

We investigate the capillary filling of three-dimensional microchannels with surfaces patterned by posts of square cross section. We show that pinning on the edges of the posts suppresses and can halt capillary filling. We stress the importance of the channel walls in controlling whether filling can occur. In particular for channels higher than the distance between adjacent posts, filling occurs for contact angles less than a threshold angle of ∼55°, independent of the height of the channel.

I. INTRODUCTION

Capillary filling, the ability of water to fill a hydrophilic channel, has been recognized since the pioneering work of Lucas and Washburn [1–3] nearly a century ago. However, investigations of capillary filling in microchannels remain interesting due to modern applications of microfluid devices. Advances in lithographic techniques mean that it is becoming increasingly feasible to fabricate microchannels with well defined surface structures on micron length scales. These have potential applications for chemical detection [4], as microreactors [5], or to build entropic traps for DNA separation [6]. Our aim in this paper is to present a numerical investigation of how posts on the surface of a microchannel affect capillary filling. Our results are relevant to the use of electrowetting to control flow in microchannels and suggest ways to overcome the difficulties of filling structured microchannels.

If a channel with hydrophilic walls comes into contact with a fluid reservoir it starts to fill as capillary forces pull the fluid into the channel. Balancing the capillary forces $(2\gamma \cos \theta_{ad})$ against the viscous drag of the entering fluid $[12\eta x(dx/dt)/H^2]$ gives an expression for the position of the advancing fluid in the channel x as a function of time t [2],

$$x^2 = \frac{\gamma H \cos \theta_{ad}}{3\eta}t, \qquad (1)$$

for a capillary of height H and infinite width. γ is the gas-liquid surface tension, η is the fluid viscosity, and θ_{ad} is the contact angle of the advancing front. This formula neglects inertial and gravitational effects (good approximations once filling is established and for channels of dimension smaller than the capillary length), assumes that the displaced fluid has zero viscosity, and neglects the slip length. These conditions are not always satisfied by simplified models used to investigation of capillary filling. However, excellent agreement between the theory and numerical results can be achieved by accounting for drag forces of the gas $[12\eta_{gas}(L-x)(dx/dt)/H^2$, where L is the length of the channel and η_{gas} is the viscosity of the gas] [7] or allowing for a slip length [8].

When the surface of a microchannel is patterned with obstacles, such as posts or ridges, the capillary filling is, in general, suppressed because of pinning on the edges of the posts. The statics of the pinning can be understood by refer-

ence to Gibbs' criterion [9]. This states that, when a fluid interface reaches an edge, it will remain pinned over the range of angles between the equilibrium contact angles on each of the surfaces bounding the edge as illustrated in Fig. 1(a). A striking consequence of Gibbs' criterion is that if there are opposing ridges across the channel it does not fill [10]. Capillary forces pull the interface until it becomes a flat surface, pinned on the edges as shown in Fig. 1(b). It cannot move down the sides of the post from this configuration and hence will remain pinned. If the meniscus is moving, however, inertial effects may allow it to overcome the pinning as it reaches the ridge. Then, as the interface moves down the channel it slows and will eventually pin at a subsequent ridge. We also note that for nanoscale roughness thermal fluctuations allow the interface to depin and advance [11].

If the ridges across the channel are replaced by separated posts capillary filling becomes possible for sufficiently low values of the contact angle. The aims of this paper are to investigate how the depinning behavior depends on the channel geometry and the contact angle and to explore the depinning mechanism in some detail. We emphasize the importance of the channel walls in controlling the depinning of the interface and we identify the way in which the interface depins for different channel geometries. Estimates are given for the contact angles at which depinning occurs.

In Sec. II we define the model we use, summarizing the equilibrium properties and the equations of motion. We then describe the geometry of the channel and list the simulation parameters of the model. In Sec. III we present our results. For two typical channels, using values of θ_{eq} which do not pin, we compare the filling rate to the similar case of a smooth channel (without obstacles), showing how posts on
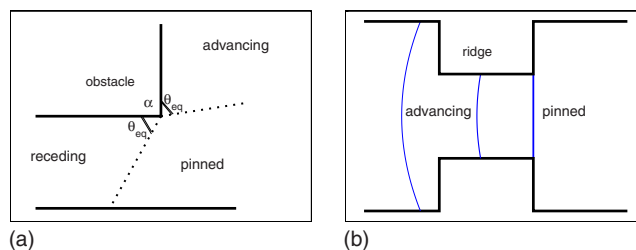

FIG. 1. (Color online) (a) When a fluid interface reaches an edge it remains pinned for a range of angles $2\pi - 2\theta_{eq} - \alpha$. (b) A fluid front, advancing from the left, remains pinned (straight line) at the edges of two opposing ridges for all contact angles.

the channel surface slow the filling. We then concentrate on the filling/pinned transition. The case in which the posts span the channel and that in which the posts do not meet across the channel are investigated in Secs. III A and III B, respectively. We find that, for high channels and long posts, the pinning-depinning threshold angle is $\theta_{th}^{\infty} \sim 55°$. The depinning is driven by the walls and is independent of the channel geometry. For narrow channels or short posts, filling is possible for higher contact angles. In Sec. III C we discuss the effect of inertia on the determination of the threshold contact angle θ_{th}^{∞}. Finally Sec. IV presents our conclusions.

II. MODEL

As we are considering micron length scales it is appropriate to describe the system using a mesoscale modeling approach. We choose to use a diffuse interface model, solved using a lattice Boltzmann algorithm [12–14], which has proven to be a useful tool to model the dynamics of fluids with moving interfaces. Of particular relevance here, Pooley *et al.* [15] demonstrated how this approach can be used to describe capillary filling in smooth microchannels. We now give details of the model, the channel geometry, and the simulation parameters used in this paper. Details of the implementation of the lattice Boltzmann method of solving the equations can be found in [15] and are not repeated here.

A. Equations of motion

We consider a binary fluid with components A and B, say, described by the free energy functional,

$$\Psi = \int_{\Omega} \left[\frac{c^2}{3} n \ln n + \frac{\kappa}{2}(\partial_{\alpha}\phi)^2 - \frac{a}{2}\phi^2 + \frac{a}{4}\phi^4 \right] + \int_{\partial\Omega} h\phi_z,$$
$$(2)$$

where n is the local total density of the A and B components ($n = n_A + n_B$), ϕ is the order parameter $\phi = n_A - n_B$, and c is the lattice velocity $c = \delta x / \delta t$, where δx is the lattice spacing and δt is the simulation time step. The first integral in Eq. (2), taken over the total volume Ω, controls the bulk properties of the system. The terms in ϕ give coexistence of phases with $\phi = \pm 1$. The energy cost of an interface between the two phases is modeled by the derivative term, with κ related to the surface tension. The term in n controls the compressibility of the fluid.

The integral over the solid-liquid interface $\partial\Omega$ in Eq. (2) accounts for the wetting properties of the solid surfaces. h is related to the equilibrium contact angle θ_{eq} by [16]

$$h = \sqrt{2\kappa a} \, \text{sgn}\left(\frac{\pi}{2} - \theta_{eq} \right) \sqrt{\cos\left(\frac{\alpha}{3}\right) \left[1 - \cos\left(\frac{\alpha}{3}\right) \right]},$$

$$\alpha = \cos^{-1}(\sin^2 \theta_{eq}), \quad (3)$$

with $\text{sgn}(x) = 1$ if $x > 0$ and $\text{sgn}(x) = -1$ otherwise.

The hydrodynamics of the fluid is described by the Navier-Stokes equations for the density ρ and the velocity field $\mathbf{v}$ together with a convection-diffusive equation for the binary order parameter ϕ,

$$\partial_t \rho + \boldsymbol{\nabla} \cdot (\rho \mathbf{v}) = 0, \quad (4)$$

$$\partial_t(\rho v_{\beta}) + \partial_{\alpha}(\rho v_{\alpha} v_{\beta}) = -\partial_{\alpha}[P_{\alpha\beta} + \eta(\partial_{\beta}v_{\alpha} + \partial_{\alpha}v_{\beta})], \quad (5)$$

$$\partial_t \phi + \boldsymbol{\nabla} \cdot (\phi \mathbf{v}) = M\nabla^2 \mu. \quad (6)$$

In Eq. (5) η is the viscosity of the fluid and in Eq. (6) M is a mobility coefficient. The pressure tensor $P_{\alpha\beta}$ and the chemical potential μ which appear in Eqs. (5) and (6), which describe the equilibrium properties of the fluid, follow from the free energy [Eq. (2)] as

$$P_{\alpha\beta} = \partial_{\alpha}\phi \frac{\delta\Psi}{\delta(\partial_{\beta}\phi)} + \delta_{\alpha\beta} \left[\phi \frac{\delta\Psi}{\delta(\phi)} + n \frac{\delta\Psi}{\delta n} - \Psi \right]$$

$$= \kappa\partial_{\alpha}\phi\partial_{\beta}\phi + \delta_{\alpha\beta} \left[\frac{c^2}{3} n + \frac{3a}{4}\phi^4 - \frac{a}{2}\phi^2 - \frac{\kappa}{2}(\partial_{\tau}\phi)^2 \right.$$

$$\left. - \kappa\phi\partial_{\tau}\partial_{\tau}\phi \right], \quad (7)$$

$$\mu = \frac{\delta\Psi}{\delta\phi} = a\phi^3 - a\phi^2 - \kappa\partial_{\tau}\partial_{\tau}\phi. \quad (8)$$

We have chosen to use a two-component binary fluid as a model system to simulate capillary filling. This is because modeling capillary filling correctly using a liquid-gas diffuse interface model is computationally demanding because of unphysical motion of the interface due to evaporation-condensation effects [7]. However our results are equally applicable to a physical system where a liquid displaces a gas as the important physical parameters are the viscosities, not the densities, of the fluid components. Therefore we shall use the natural terminology "liquid" and "gas" for the displacing and displaced fluid from now on.

B. Simulation geometry

Figure 2 reports the channel geometry which we use in this paper. Two reservoirs, of liquid and gas, which are in contact to equalize the pressure, are connected to a channel, running along x, with walls decorated by equispaced rectangular posts. The relevant geometric parameters are the channel height H (measured from wall to wall), the distance between the top of two posts on opposing walls H_{eff}, the distance between two obstacles across the channel L, and the cross section of the posts which we choose to be square with side of length D.

C. Simulation parameters

All the quantities reported in this paper are expressed in units of δx, the lattice spacing, and δt, the time step and hence $c = 1$. We simulate channels with one, two, or three rows of posts corresponding to lengths (in the x direction; see Fig. 2) L_x from 80 to 200 lattice spacing. In the y direction we employ periodic boundary condition and sizes L_y from 60 to 170, while $H = L_z$ spans from 30 to 100. For the reservoirs we use the same $L_{y,\text{res}} = L_y$ while in the z direction we use periodic boundary conditions with $L_{z,\text{res}}$ two or three
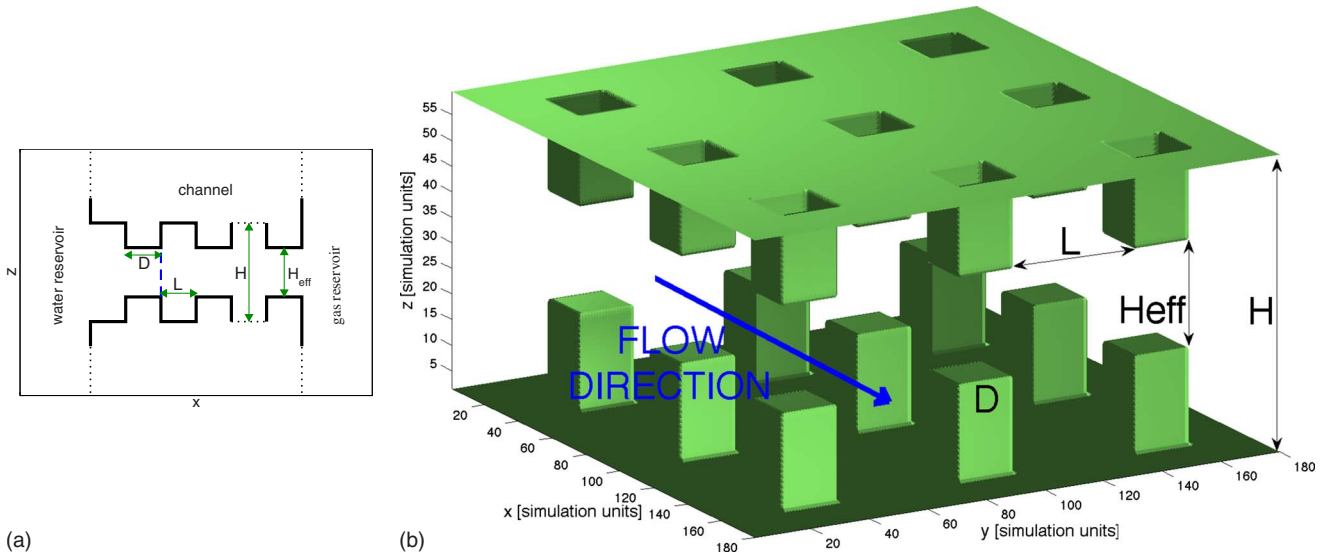
FIG. 2. (Color online) Structure and parameters of the channel. The fluid flows from left to right along the x axis. H is the height of the channel, H_{eff} is the distance between the tops of the posts, D is the dimension of the square posts, and L is the distance between the posts. (a) is a cross section in the x-z plane and (b) is a three-dimensional view of the channel geometry.

times L_z. The x length of the reservoir $L_{x,res}$ is approximately half the channel length L_x. For the free energy [Eq. (2)], the bulk phases ($\phi=1$ and $\phi=-1$) are interpolated by an interface with a profile which is well approximated by $\phi = \tanh(x/\sqrt{2}\xi)$ (with $\xi=\sqrt{k/a}$) and with a surface tension equals $\gamma=\sqrt{8ka/9}$. Here we use $a=0.04$ and $k=0.02$. These values give an interface width of order four lattice Boltzmann nodes which is much smaller than the typical size of the posts used. The viscosity η and the mobility coefficient M appearing in the hydrodynamic equations [Eqs. (5) and (6)] are related to the relaxation time in the lattice Boltzmann algorithm [12]. We use $M=0.25$. For the gas viscosity $\eta_{gas}=0.033$, while for the liquid (unless specified) $\eta_{liq}=0.83$. Both the gas and liquid densities are set to 1.

III. RESULTS

In a typical simulation we start with a configuration in which the liquid-gas interface has advanced to the end of the first row of posts as indicated by the broken line in Fig. 2. If

the contact angle is not too large, the interface moves through the channel, driven by the capillary force. If the filling fluid overcomes the first row of obstacles, we have verified it depins from the second row too. We have also used starting configurations with empty channels, finding no differences in the filling or pinned phase diagram.

Figure 3 shows the position of the advancing front (in the middle and near the walls of the channel) as a function of time for two typical geometries and for contact angles which do not pin. It is immediately apparent that the flow profile is very different to that of a smooth channel $H_{eff}=H$. Three regimes are present. When the advancing fluid reaches the beginning of the obstacles (dotted lines in Fig. 3) it accelerates because of the increase in the capillary force due to more wettable surface provided by the obstacles. When the front reaches the end of the obstacles it remains pinned for a certain time during which it is almost at rest. When finally it depins it restarts filling the channel with a Lucas-Washburn-like law [Eq. (1)] but with a reduced velocity (the "decelerated" regime compared to the smooth channel in Fig. 3). This
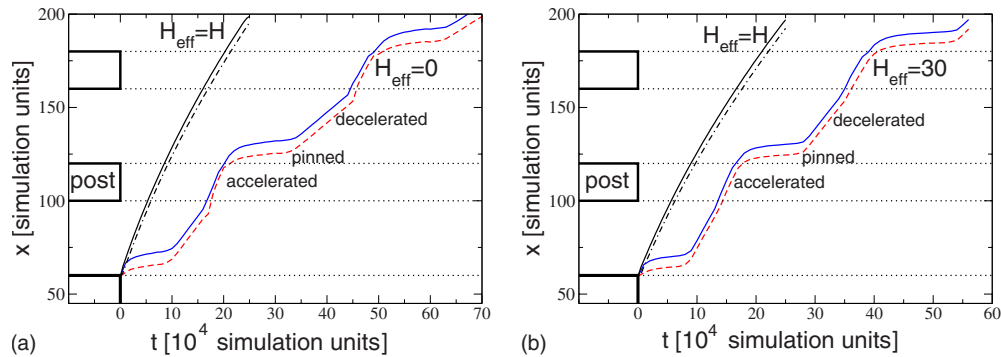

FIG. 3. (Color online) Position x of the advancing front for (a) $D=20$, $L=40$, $H_{eff}=0$, $H=40$, $\theta_{eq}=55°$ and (b) $D=20$, $L=40$, $H_{eff}=30$, $H=50$, $\theta_{eq}=60°$ as a function of time t. The positions of the advancing front near the wall (full line) and in the middle of the channel (broken line) are compared. We compare the filling rate for the same channel without posts ($H_{eff}=H$).
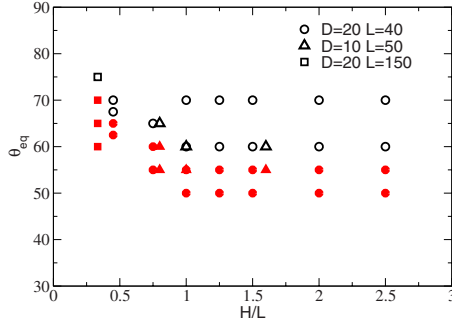
FIG. 4. (Color online) Filling/pinning transition for the $H_{eff}=0$ geometry (posts that span the channel; see Fig. 2). Open symbols are simulations in which the front is pinned while full symbols correspond to simulations in which the channel is filled. For $H/L \gtrsim 1$ the filling-pinning transition happens for a threshold angle of $\sim 55°$, while for $H/L \lesssim 1$ the transition is possible for a range of equilibrium contact angles which increases with decreasing H/L.

happens because the drag force is now larger due to the presence of the obstacles within the displacing viscous fluid. We observe that the "accelerated" and decelerated regimes are more obvious for $H_{eff}=0$ because the post surface is bigger than for $H_{eff}=30$.

For the parameters considered in Fig. 3 the front is finally able to depin from each of the obstacles to move down the channel, but for lower contact angles it remains pinned. We next look in more detail at the pathways for depinning.

A. $H_{eff}=0$

We first consider geometries in which the posts span the channel ($H_{eff}=0$ in Fig. 2). Figure 4 summarizes results which distinguish the cases where the interface is pinned on the posts from those where it can advance along the channel for a range of geometric parameters (H, L, and D, defined in Fig. 2) and equilibrium contact angles θ_{eq}.

At high θ_{eq} the front remains pinned. However, at lower θ_{eq} the meniscus can overcome Gibb's pinning and the channel fills. This is due to the presence of walls bounding the channel. By advancing along the walls the meniscus is able to reach the angle it needs to move across the face of the posts. This is illustrated in Fig. 5 for different aspect ratios of the channel.

Two different regimes are apparent in Fig. 4. For $H/L \gtrsim 1$ the boundary between contact angles that allow filling and those that do not is independent of H/L occurring at an angle, which we shall denote θ_{th}^{∞}, $\sim 55°$. For $H/L \lesssim 1$, however, the transition angle is not constant but increases with decreasing H/L.

Figure 5 compares the way in which the front depins from the posts in each of the two regimes. For $H/L \gtrsim 1$ [Fig. 5, column (a)] the walls act independently. The menisci from two neighboring gaps first meet at the walls and then the advancing front covers the posts, moving from the walls toward the center of the channel. Hence the contact angle below which depinning proceeds, θ_{th}^{∞}, is independent of H/L.

Further evidence is provided for this by Fig. 6 which shows how the meniscus advances along the wall for differ-

ent values of H and at fixed L. The profiles are nearly independent of H as long as the front remains pinned. Without obstacles, the Lucas-Washburn law predicts a velocity proportional to H [Eq. (1)], so that the profiles in Fig. 6 would be well separated in a smooth channel.

We stress the importance of the walls even in the limit $H \rightarrow \infty$. Even for a very high channel depinning will occur at θ_{th}^{∞} and will proceed as in Fig. 5, column (a) (except that it will take more time to wet the posts). However, without any walls the advancing fronts will remain pinned at the obstacles and flat as in Fig. 1(b).

For $H/L \lesssim 1$, however, depinning occurs for contact angles greater than θ_{th}^{∞}. This is because the walls are sufficiently close that the interface moves in a concerted way across the channel. Therefore, once the menisci have advanced along the surfaces sufficiently far for depinning to occur, the interface depins along all of a post at the same time, and the posts are wet from the sides. As H/L decreases the two surfaces more easily deform the interface and hence depinning can take place at a higher contact angle. This agrees with analytic results showing that, in the $H/L \rightarrow 0$ limit, the interface depins for all hydrophilic contact angles [17] and can be understood using a free energy argument. The free energy gain in deforming the advancing interface scales like the area of the gas-liquid interfaces and goes to zero as H for $H \rightarrow 0$. However the loss in free energy due to the wetting of the walls remains constant for $H \rightarrow 0$. As a consequence the interface will advance for any $\theta_{eq} < 90°$ for sufficiently small H.

We expect the phase diagram to depend only on H/L and to be independent of D as, once the front has started to depin, the interface will continue moving across the post until it covers it. Indeed, using $L=40$ we repeated simulations for $D=30$ ($H=60,80$) and $D=40$ ($H=60,80$) finding, again, a depinning transition compatible with θ_{th}^{∞}. On the other hand we observed a weak dependence of θ_{th}^{∞} on L. We repeated simulations for $L=30$, $D=30$, and $H/L=20$, 30, 50, 80, 100, and 120. θ_{th}^{∞} was again independent of H/L for $H/L \gtrsim 1$, but placed between $50°$ and $55°$, while for $L=40$ (Fig. 5) $\theta_{eq}=55°$ fills the channel. In Sec. III C we show that the dependence of θ_{th}^{∞} on L is related to inertial effects.

B. $H_{eff}>0$

In this section we describe the behavior for the more general case $H_{eff}>0$ when the posts do not reach all the way across the channel. We will consider the $H/L \gtrsim 1$ geometry where the interface depins from posts with $H_{eff}=0$ by a transition at θ_{th}^{∞}, driven by depinning initiated at the walls. For $H_{eff}>0$ filling the channel should be easier.

Figure 7 shows pinned configurations of the meniscus near the channel wall for different values of H_{eff}, keeping the other geometric parameters fixed, and for $\theta_{eq}=60°$. For $H_{eff}=0$ this corresponds to a pinned configuration. The effect of increasing H_{eff} is to increase the contact angle at the edge of the post. When this angle exceeds the equilibrium contact angle ($\theta_{eq}=60°$ in Fig. 7) then, as predicted by Gibbs' criterion, the front depins. For the parameters of Fig. 7 this happens for $H_{eff}=40$ (not reported in the figure).
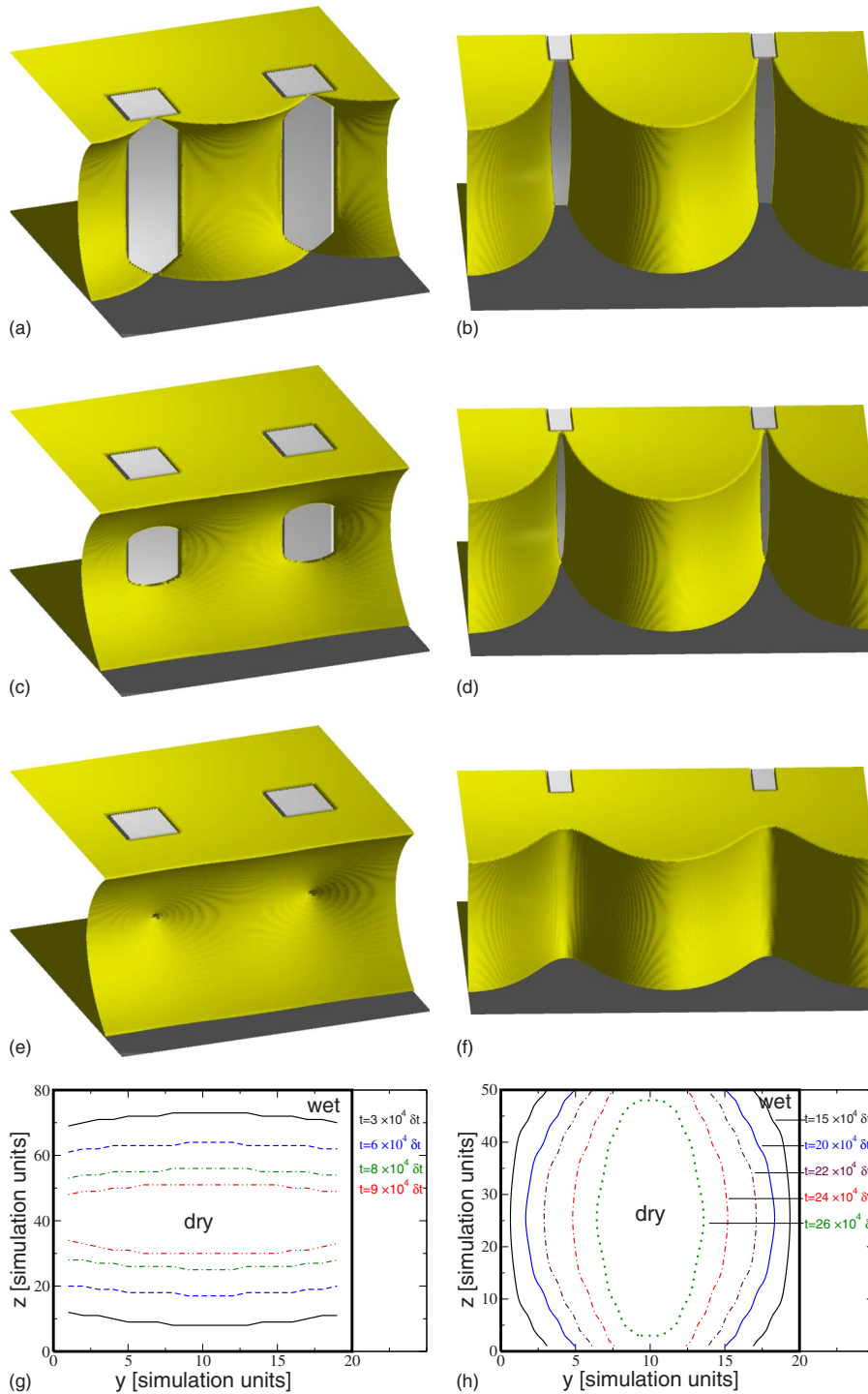
FIG. 5. (Color online) Depinning path ways for $H_{\mathrm{eff}}=0$: (a) $H/L>1$ ($D=20$, $L=40$, $H=80$, $\theta_{\mathrm{eq}}=50°$) and (b) $H/L<1$ ($D=20$, $L=150$, $H=50$, $\theta_{\mathrm{eq}}=70°$). The first three rows are three-dimensional views of the advancing front (aspect ratios not to scale) and the fourth row shows the position of the advancing front on the face of the posts as a function of time during depinning. Note that for $H/L \gtrsim 1$ (a) the fluid wets the posts from the walls of the channel, whereas for $H/L \lesssim 1$ (b) the fluid advances from the sides of posts.

For $H_{\mathrm{eff}} \lesssim H/2$, the angle the meniscus makes with the edge of the post does not change significantly. For this reason, at low values of H_{eff} the threshold equilibrium contact angle is almost the same as in the $H_{\mathrm{eff}}=0$ case (i.e., $\approx \theta_{\mathrm{th}}^{\infty}$). However the meniscus advances significantly from its position at $H_{\mathrm{eff}}=0$ when H_{eff} becomes comparable to H. This can be explained by considering the shape of the pinned inter-face. If $H_{\mathrm{eff}}=0$ and $H/L \gtrsim 1$, the pinned front is almost flat in the middle of the channel with significant deviations only near the walls. If H_{eff} is small enough that the gap does not overlap with the wall regions, then it will not perturb the interface compared to the $H_{\mathrm{eff}}=0$ configuration. On the other hand for large H_{eff}, the end of the posts will lie within the wall region and there will be significant deformation of the
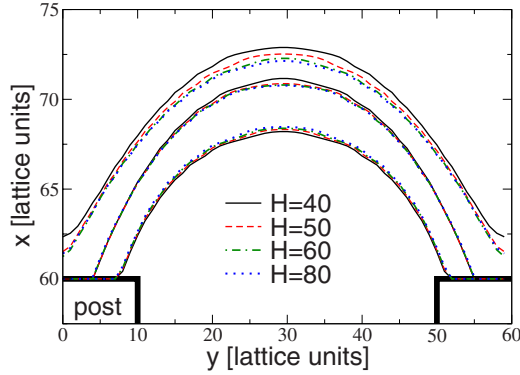
FIG. 6. (Color online) Position of the depinning front near the walls (at $z=2$) as a function of time (for $t=1$, 2 and 3×10^4 lattice Boltzmann time steps) for $\theta_{\mathrm{eq}}=50°$ and several H so that $H/L \gtrsim 1$ with $L=40$.

pinned front, compared to the $H_{\mathrm{eff}}=0$ case, and a threshold equilibrium contact angle different to $\theta_{\mathrm{th}}^{\infty}$.

For several channels ($D=20$, $L=40$, $H=40$, 50, 60, 70, and 80) we have verified that at low H_{eff} the front remains pinned at $\theta_{\mathrm{eq}}=60° > \theta_{\mathrm{th}}^{\infty}$, as in the $H_{\mathrm{eff}}=0$ case, while at high enough H_{eff}, $\theta_{\mathrm{eq}}=60°$ can fill the channel. We were never able to observe filling for $\theta_{\mathrm{eq}}=65°$, but we do not exclude that at high enough H_{eff} (which would require a larger simulation box to properly resolve the small height of the posts) this can happen.

Results summarizing the threshold in H_{eff} above which $\theta_{\mathrm{eq}}=60°$ fills are reported in Fig. 8. Having fixed D and L, we use H_{eff}/H and H/L as control parameters. At low value of H/L the filling for $\theta_{\mathrm{eq}}=60°$ occurs for values of H_{eff}/H greater than 0.5 (see full circles). Increasing H/L higher values of H_{eff}/H are needed to achieve filling at $60°$ because the length of flat interface in the middle of the channel increases with increasing H.

At small values of H_{eff} (for which $\theta_{\mathrm{eq}}=60°$ does not fill) the depinning route is the same as for $H_{\mathrm{eff}}=0$. This is shown in the first column of Fig. 9. As the meniscus advances near the walls of the channel the interface between the posts remains almost completely flat. The posts are wet, as before, from the channel walls toward the center. This is not the case
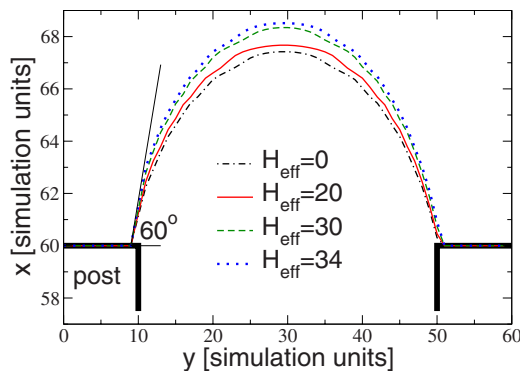

FIG. 7. (Color online) Position of the pinned meniscus near the walls ($z=2$) for $H=60$, $D=20$, $L=40$, $\theta_{\mathrm{eq}}=60°$, and four values of H_{eff}. Increasing H_{eff} the contact angle at the edge of the post is increased until the depinning threshold is reached (for $H_{\mathrm{eff}}=40$).
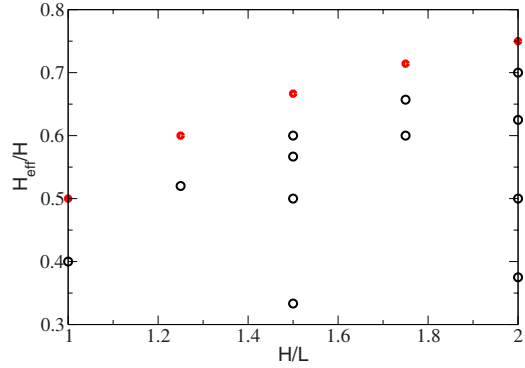

FIG. 8. (Color online) Full symbols denote values of H_{eff} (with $D=20$, $L=40$, and $H=40$, 50, 60, 70, and 80) for which the channel will fill at an equilibrium contact angle $\theta_{\mathrm{eq}}=60°$. Empty circles correspond to interfaces that remain pinned at $\theta_{\mathrm{eq}}=60°$ as in the case $H_{\mathrm{eff}}=0$.

for larger value of H_{eff} (full symbols in Fig. 8). In Fig. 9, column (b), the advancing front does not remain pinned in the middle of the channel but the posts are wet from their ends and sides toward the walls.

C. Inertial effects

In performing the simulations we found that inertial effects made it difficult to determine the exact contact angle at which depinning occurs. If the front reaches the free energy minimum which corresponds to pinning with a residual kinetic energy it can overshoot and hence depin, and it is not possible to entirely eliminate this effect without prohibitively long simulations. Indeed in a physical system the front will approach the posts with a finite velocity and whether it will pin will be a balance between θ_{eq} and the extent to which the front has been slowed by the viscous drag in the channel.

To demonstrate the effects of inertia close to the depinning transition we investigated filling a channel with $D=20$, $L=40$, $H=60$, $H_{\mathrm{eff}}=0$, and $\theta_{\mathrm{eq}}=55°$, from the starting configuration shown in Fig. 2, for three different liquid viscosities. Figure 10 shows the position of the advancing front as a function of time for each case. At early times lower viscosities give slightly higher speeds. However, the higher viscosity fluids gain more energy from the walls and have sufficient inertia to move fast the pinning position for this contact angle whereas, at least on the time scale of the simulation, the lowest viscosity fluid remains pinned. As anticipated in Sec. III A, inertial effects are also responsible for the dependence of $\theta_{\mathrm{th}}^{\infty}$ on L, which controls the amount of water advancing between two posts (or equivalently the scale of the system).

We tried to better determine the position of $\theta_{\mathrm{th}}^{\infty}$ repeating simulations in which θ_{eq} was gradually decreased (by $0.5°$ each 10^5 time steps) to better reproduce a quasistatic relaxation of the interface. For a channel with $L=30$ we obtained $\theta_{\mathrm{th}}^{\infty}=52.5° \pm 0.5°$. However this estimate is very difficult because of the flatness of the free energy profile and the very slow interface velocities.

We stress that, for angles near depinning, inertial effects depend primarily on the way in which the interface is pulled
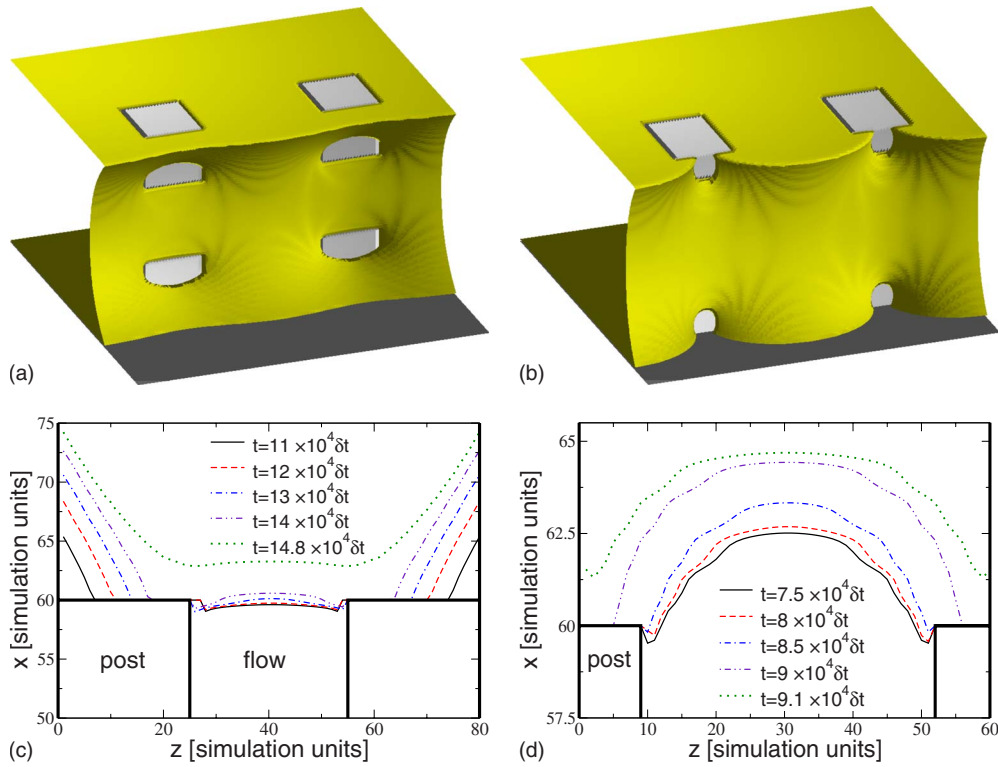
FIG. 9. (Color online) Depinning mechanism for (a) $H=80$, $H_{eff}=30$, $L=40$, and $\theta_{eq}=55°$ and (b) $H=60$, $H_{eff}=40$, $L=40$, and $\theta_{eq}=60°$. In the first row we report three-dimensional interface profiles during depinning, while in the second row the position of the advancing front along a section taken through the center of a post at different times. In (b) the face of the post is wet both from its ends and sides.

beyond the end of the posts by the surface but not on its initial position within the microchannel. Hence we expect that this is not just an artifact of the simulations, but that similar inertial effects will occur in experimental systems.

IV. DISCUSSION

As microfabrication techniques become standard it is becoming possible to design microchannels with complicated internal geometries that may prove useful in controlling fluid behavior. As a step toward understanding how fluids move in such channels we have investigated capillary filling in microchannels patterned by regularly spaced square posts. A con-
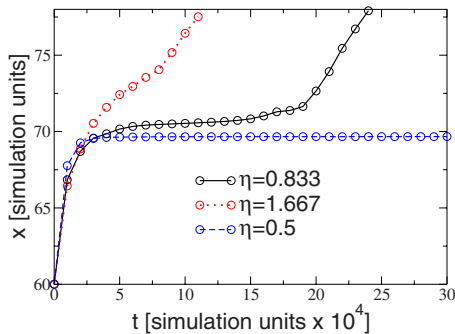

FIG. 10. (Color online) Position of the maximum of the advancing front near the wall ($z=2$) as a function of time for $D=20$, $L=40$, $\theta_{eq}=55°$, and three different values of the viscosity η.

sequence of Gibbs' criterion is that ridges that face each other across a channel will always pin a slowly moving interface. We show that, if the ridges are replaced by posts, the interface is able to depin for sufficiently small contact angles. This is because the meniscus can advance along the surfaces of the channel between the posts, thus allowing depinning to occur.

For posts which span the channel and for a ratio of channel height to distance between the posts $H/L \gtrsim 1$ the depinning threshold θ_{th}^{∞} is independent of H/L because the two surfaces of the channel act independently. θ_{th}^{∞} lies between $55°$ and $60°$ and the posts are wet from the surfaces toward the center of the channel. For $H/L \lesssim 1$ the threshold contact angle increases with decreasing H/L as the surfaces act cooperatively to reduce interface curvature across the channel. Here the posts primarily wet from their sides to their centers.

In the general case in which the posts on opposing sides of the channel are separated by a distance H_{eff} two regimes are present for $H/L \gtrsim 1$. At low H_{eff} the filling/pinned transition is similar to that for $H_{eff}=0$, with a threshold value of the equilibrium contact angle around θ_{th}^{∞} and posts which wet from the wall to the center of the channel. For high enough H_{eff}, however, the threshold equilibrium contact angle for depinning increases, and the posts can also wet from the center of the channel toward the walls during depinning. These results are in agreement with [10], where channels with fixed H and H_{eff} and several L were considered. In particular in the range $H/L \gtrsim 1$, a contact angle threshold compatible with θ_{th}^{∞} was observed. On increasing the value of L (i.e., exploring the $H/L \lesssim 1$ regime), filling at higher θ_{eq}

was found, in agreement with our $H_{\text{eff}}=0$ results.

We have concentrated mainly on the quasistatic situation where inertia is neglected and therefore our threshold values are relevant to a very slowly moving interface. We have, however, shown that close to the threshold even tiny interface velocities can aid depinning. It will now be interesting to investigate the more general case of a moving interface and assess the extent to which dissipation at the posts can slow and eventually pin the interface for a range of contact angles.

The contact angle of a fluid within a microchannel can rather easily be varied by applying an electrowetting poten-tial. This opens the possibility of controlling the fluid motion by switching θ_{eq} in and out of the pinning regime [18]. This is of particular interest in the large H/L regime because the threshold equilibrium contact angle is well approximated by $\theta_{\text{th}}^{\infty}$, independent of the channel geometry.

[1] R. Lucas, Kolloid-Z. **23**, 15 (1918).

[2] E. W. Washburn, Phys. Rev. **17**, 273 (1921).

[3] J. M. Bell and F. K. Cameron, J. Phys. Chem. **10**, 658 (1906).

[4] D. Janasek, J. Franzke, and A. Manz, Nature (London) **442**, 374 (2006).

[5] W. Ehrfeld, V. Hessel, and H. Lowe, *Microreactors: New Technology for Modern Chemistry* (Wiley-VCH, Weinheim, 2000); A. J. deMello, Nature (London) **442**, 394 (2006).

[6] J. Han and H. G. Craighead, Science **288**, 1026 (2000).

[7] F. Diotallevi, L. Biferale, S. Chibbaro, G. Pontrelli, F. Toschi, and S. Succi, Eur. Phys. J. Spec. Top. **171**, 237 (2009).

[8] D. I. Dimitrov, A. Milchev, and K. Binder, Phys. Rev. Lett. **99**, 054501 (2007).

[9] J. W. Gibbs, *Scientific Papers 1906* (Dover, New York, 1961); P. Concus and R. Finn, Acta Math. **132**, 177 (1974).

[10] H. Kusumaatmaja, C. M. Pooley, S. Girardo, D. Pisignano, and J. M. Yeomans, Phys. Rev. E **77**, 067301 (2008).

[11] S. Chibbaro, E. Costa, D. Dimitrov, F. Diotallevi, A. Milchev, D. Palmieri, G. Pontrelli, and S. Succi, Langmuir **25**, 12653 (2009); S. Chibbaro, L. Biferale, K. Binder, D. Dimitrov, F. Diotallevi, A. Milchev, and S. Succi, J. Stat. Mech.: Theory Exp. 2009, P06007.

[12] S. Succi, *The Lattice Boltzmann Equation for Fluid Dynamics and Beyond* (Oxford University Press, Oxford, 2001).

[13] J. M. Yeomans, Physica A **369**, 159 (2006).

[14] M. R. Swift, E. Orlandini, W. R. Osborn, and J. M. Yeomans, Phys. Rev. E **54**, 5041 (1996).

[15] C. M. Pooley, H. Kusumaatmaja, and J. M. Yeomans, Phys. Rev. E **78**, 056709 (2008).

[16] J. W. Cahn, J. Chem. Phys. **66**, 3667 (1977).

[17] S. Richardson, Eur. J. Appl. Math. **12**, 665 (2001); V. A. Bogoyavlenskiy and E. J. Cotts, Phys. Rev. E **69**, 016310 (2004); G. L. Vasconcelos, *ibid.* **76**, 038301 (2007).

[18] B. M. Mognetti and J. M. Yeomans (unpublished).